Journal of Quantitative Spectroscopy & Radiative Transfer 162 (2015) 154–163

Contents lists available at ScienceDirect

Journal of Quantitative Spectroscopy & Radiative Transfer

journal homepage: www.elsevier.com/locate/jqsrt

Scattering of a plane electromagnetic wave by a generalized Luneburg sphere–Part 1: Ray scattering

James A. Lock [a,*], Philip Laven [b], John A. Adam [c]

[a] Physics Department, Cleveland State University, Cleveland, OH 44115, USA
[b] 9 Russells Crescent, Horley RH6 7DJ, United Kingdom
[c] Department of Mathematics and Statistics, Old Dominion University, Norfolk, VA 23529, USA

ARTICLE INFO

Article history:
Received 2 October 2014
Received in revised form
6 February 2015
Accepted 9 February 2015
Available online 20 February 2015

Keywords:
Scattering
Radially-inhomogeneous sphere
Geometrical optics

ABSTRACT

We calculated scattering of an electromagnetic plane wave by both a radially-inhomogeneous particle and bubble, the square of whose refractive index profile is parabolic as a function of radius. Depending on the value of the two adjustable parameters of the parabola, the particle or bubble can have either a refractive index discontinuity at its surface, or the refractive index can smoothly merge into that of the exterior medium. Scattering was analyzed in ray theory, and various novel features of the scattering, including the details of the curved ray paths, transmission rainbows, and near-critical-angle scattering were apparent and were contrasted with their behavior for scattering by a homogeneous sphere.

1. Introduction

Much has been learned about the interaction of electromagnetic radiation with macroscopic matter by examining scattering of an incident plane wave or a transversely localized beam by a homogeneous dielectric spherical particle. It is also of both theoretical and practical interest to understand the details of scattering of electromagnetic radiation by a radially-inhomogeneous sphere. In this new setting, one would expect to revisit all the familiar phenomena encountered in scattering by a homogeneous sphere. But, in addition, either new phenomena might occur which are impossible for the more specialized geometry of a homogeneous sphere, or familiar phenomena may occur in totally new ways. Toward that end, in this paper, we study scattering of a plane wave by a particular type of radially-inhomogeneous sphere called a generalized Luneburg lens (GLL). We do this not because of the practical utility of these particles or their ubiquity in nature (although manufactured Luneburg lenses are used as directional antennas for microwaves [1]), but because every aspect of the scattering is analytically soluble in ray theory. This is of considerable importance given the paucity of available analytic solutions for radially inhomogeneous media [2]. The general phenomena we encounter are not specific to scattering by a GLL, but are expected to occur to some degree for scattering by a wide variety of generically similar radially-inhomogeneous profiles. Previous studies of scattering by a Luneburg lens and some of its variants are analyzed in [1,3–11].

Depending on the value of the two parameters describing the GLL, 15 distinct scattering geometries are possible. In this paper, we examine 11 of these geometries using ray theory, which in most cases gives a close approximation to wave scattering in the small wavelength limit. The body of this paper is organized as follows. In Section 2, we enumerate the 11 different GLL geometries to be examined and preview a few of their more interesting behaviors. In Section 3, we determine various properties of ray scattering of particle-like GLLs, concentrating on the deflection

* Corresponding author.
E-mail address: j.lock@csuohio.edu (J.A. Lock).

http://dx.doi.org/10.1016/j.jqsrt.2015.02.013
0022-4073/

angle as a function of the angle of incidence, the shape of the curved ray path inside the GLL, the optical path length from a ray's entrance plane to its exit plane, and the scattered intensity. In Section 4, we do the same for bubble-like GLLs. In Section 5, we briefly comment on our more unusual, significant, and interesting results. To complete our study of GLLs, the most interesting scattering features appearing in ray theory are examined in a companion paper [12] using wave theory by approximating the radially-inhomogeneous sphere by a finely-stratified multi-layer sphere, and in the time domain by considering scattering of a femtosecond pulse by the sphere.

2. Refractive index profile

We consider an electromagnetic plane wave of amplitude E_0, wavelength λ, wave number $k=2\pi/\lambda$, linearly polarized in the x direction, and propagating in the $+z$ direction in an external medium of refractive index 1. The plane wave is scattered by a GLL of radius a whose center is at the origin of coordinates, and has the radially inhomogeneous refractive index profile

$$N(r)=\left[2B-C\left(r/a\right)^2\right]^{1/2}, \tag{1}$$

where B and C are the positive or negative constants. This has previously been called the parabolic distribution [13] because the dielectric constant of the sphere varies parabolically in r. The (B, C) parameter space of Eq. (1) is shown in Fig. 1.

For the case of $C>0$, the GLL is particle-like in region η and on the line γαβ, for which

$$2B\geq C+1. \tag{2}$$

This portion of (B, C) space is characterized by the refractive index being a decreasing function of r with $N(a)\geq 1$. Since $2B>C+1$ in region η, $N(a)>1$ and there is a refractive index discontinuity at the sphere surface. As a result, the GLL is said to have a hard edge. Since $2B=C+1$ on line γαβ, $N(a)=1$ and the GLL is said to be edgeless [3]. A GLL represented by point α is the original edgeless Luneburg lens for which an incident plane wave focuses on the sphere axis at its back surface [3]. The points on the line segments β and γ represent the edgeless modified Luneburg lenses studied in [9–11] which were previously found to have either no transmission rainbows (hereafter called bows because the Luneburg spheres have nothing to do with rain) or one transmission bow, respectively. The points in region η represent hard edge particle-like GLLs that will be shown in Section 3 to have either zero or two transmission bows. In region ν the refractive index of the GLL is a decreasing function of r with and $0\leq N(r)\leq 1$ for $0\leq r\leq a$. Since $N(a)\leq 1$, it resembles a radially inhomogeneous air bubble in water, and is said to be bubble-like.

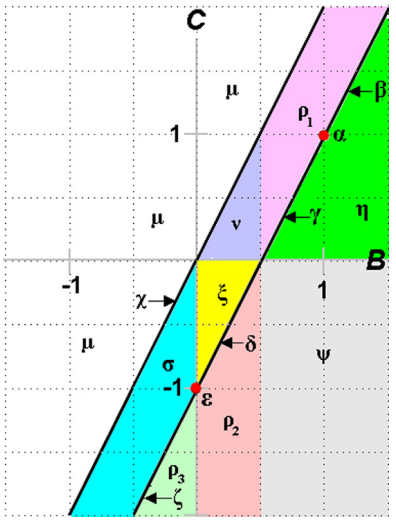

Fig. 1. (B, C) parameter space.

For the case of $C<0$ and

$$C\leq 2B\leq C+1, \tag{3}$$

corresponding to regions ξ and σ and line δεζ in Fig. 1, the GLL is bubble-like with $N(r)$ being an increasing function of r. Depending on whether $N(a)=1$ or $N(a)<1$ the GLL is either edgeless or has a hard edge. Points on the line segments δ and ζ represent edgeless bubble-like modified Luneburg lenses that will be seen in Section 4 to have either one or zero transmission bows, respectively. The GLL represented by point ε is an edgeless bubble-like sphere whose refractive index profile reduces to $N(r)=r/a$. Similarly, points in region ξ represent hard edge bubble-like GLLs that will also be shown in Section 4 to have either zero or two transmission bows. In region ψ the GLL is particle-like with $N(r)$ being an increasing function of r. Points in region σ are bubble-like GLLs that will be shown to have no transmission bows, but have quite a different ray trajectory inside the bubble than is the case in region ξ. This is due to the fact that in region σ the refractive index changes from positive to imaginary at some radius inside the sphere. Certain features of the ray scattering of a GLL turn out to be discontinuous at points α and ε from their behavior on the adjacent line segments β and γ, and δ and ζ, respectively. Similarly, certain ray scattering features on the line segments β, γ, δ, ζ have discontinuities from their behavior in the adjacent regions η, ξ, and σ. These points will be addressed more completely in Section 4.

Lastly, the line segment $0<B<1/2$, $C=0$ describes a homogeneous bubble and the line segment $1/2<B$, $C=0$ describes a homogeneous particle which can be analyzed using Lorenz–Mie theory. The regions ρ_1, ρ_2, and ρ_3 in Fig. 1 have $N(r)>1$ for some radii inside the sphere and $N(r)<1$ for other radii. This geometry has a mixed character, which could, in principle, be realized by placing a particle-like GLL in an external medium whose refractive index is intermediate between $N(0)$ and $N(a)$, and then considering the relative refractive index. These mixed cases will not be considered here. A GLL in region μ, for which $N(a)$ is imaginary will also not be considered here. For $C>0$ this would correspond to an incident wave becoming evanescent as it crosses the sphere surface, and remaining so a certain distance inside the sphere, resembling a tunneling situation.

We label the various scattering process according to the notation for the Debye series decomposition of the partial

wave scattering amplitudes for a homogeneous spherical particle [14–16]. The combination of diffraction and external reflection is denoted by $p=0$, direct transmission is $p=1$, and transmission following $p-1$ internal reflections is $p\geq 2$. Neither internal nor external reflection can occur at the surface of an edgeless GLL. As a result, the only scattering processes are diffraction and transmission. In contrast, all Debye series scattering processes occur for GLLs having a hard edge.

In the context of ray theory, the path of a geometrical light ray within a radially-inhomogeneous medium is curved, and is identical to the curved trajectory of a point mass of energy E in the external potential $U(r)$ of a conservative force field centered at the origin and given by [17]

$$U(r)=-E\left[N^2(r)-1\right]. \tag{4}$$

The force field is attractive when $C>0$, and it is repulsive when $C<0$. Thus one can use the intuition obtained from this mechanical analogy to understand the details of the curved ray path in the corresponding optical problem.

3. Ray scattering by a Luneburg sphere having $C>0$

3.1. Deflection angle and properties of the ray path

We first consider the case $C>0$. Let θ_i be the angle of incidence of an incoming ray at the sphere surface, and Θ be the deflection angle of the corresponding exiting ray. We use the sign convention that $\Theta>0$ if the incident ray propagates above the horizontal z axis and the outgoing deflected ray propagates below the z axis as in Fig. 2 below. Similarly, $\Theta<0$ if both the incident and outgoing deflected ray propagate above the z axis as in Fig. 5 below. The deflection angle for a specific Debye process is denoted by Θ_p. Transmission of a ray through the GLL is calculated using the formula for the deflection of a point particle in an arbitrary potential $U(r)$ [18] or the curvature of a ray in a medium of arbitrary refractive index [19], applied to the special case of the external potential of Eq. (4). For $C>0$, the transmission deflection angle Θ_1 is constrained to be in the interval $0^\circ\leq\Theta_1\leq 180^\circ$. This is evident in Fig. 2 for the special case $B=1.5$, $C=2$ on line segment β in Fig. 1. Using the formula for Θ_1, the deflection angle for transmission following $p-1$ internal reflections for arbitrary $p\geq 1$ of a GLL represented by a point in regions η or ν of Fig. 1 is found to be

$$\Theta_p=(p-2)\pi/2+2\theta_i+p\ \arcsin\left\{\left[B-\sin^2(\theta_i)\right]\Big/\left[B^2-C\ \sin^2(\theta_i)\right]^{1/2}\right\}. \tag{5}$$

In the particle-like region η, Eq. (5) is valid for $0^\circ\leq\theta_i\leq 90^\circ$, while in the bubble-like region ν it is valid only for $0^\circ\leq\theta_i\leq\theta_i^C$ where θ_i^C is the critical angle for total external reflection given by

$$\sin\left(\theta_i^C\right)=(2B-C)^{1/2}. \tag{6}$$

In region ν, the deflection angle $\Theta(\theta_i)$ approaches $\Theta(\theta_i^C)$ with infinite slope as θ_i approaches θ_i^C. In the context of ray theory, incident rays with $\theta_i\geq\theta_i^C$ are totally externally reflected at the surface and never enter the GLL. An identical effect occurs for scattering of a plane wave by a homogeneous air bubble in water [20–22].

In the mechanical analogy to $C>0$, since the refractive index is a decreasing function of r, a point mass moves under the influence of an attractive external potential. It accelerates toward the force center as it passes its location, and the trajectory curves around the origin. Consistent with this qualitative observation, the shape of a transmission ray path inside the particle-like GLL of region η and the bubble-like GLL of region ν is found to be a section of an ellipse, as is shown in Fig. 2 and is parameterized as follows. Consider the z axis to be horizontal and the ρ axis (i.e. x or y axis) to be vertical. The axes z' and ρ' are rotated clockwise with respect to the z, ρ axes by the (negative) angle $-\Theta_1/2$ (i.e. they are rotated counterclockwise). After much algebra, the elliptical path of a transmitted ray inside the GLL is given by

$$\rho'^2/\left[(u-v)a^2\right]+z'^2/\left[(u+v)a^2\right]=1, \tag{7}$$

where

$$u=B/C \tag{8a}$$

$$v=\left[B^2-C\ \sin^2(\theta_i)\right]^{1/2}/C. \tag{8b}$$

The point of closest approach of a ray to the origin along its curved path is given by $z'=0$ in Eq. (7). The greatest difference between the ray paths in regions η and ν is that since $N(a)>1$ in region η, the ray path refracts at the sphere surface toward the sphere center before it continues to smoothly curve in the same sense once inside the GLL. On the other hand since $N(a)<1$ in region ν the ray path initially refracts at the sphere surface away from the sphere center before it smoothly curves toward the center thereafter.

The integral of ds along the elliptical ray path is an elliptic integral of the second type, but the integral of the optical path length Nds for the refractive index profile of Eq. (1) is analytically soluble. The optical path length between a ray's entrance and exit planes, which are perpendicular to the ray's direction in the exterior medium and tangent to the sphere surface, is

$$L_p=a\left[2-2\cos(\theta_i)+pS\right] \tag{9}$$

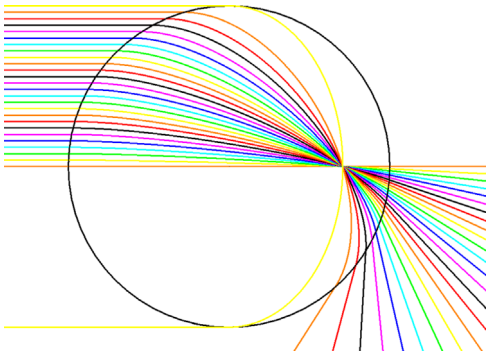

Fig. 2. Ray tracing for a GLL with $B=1.5$ and $C=2$ (on line segment β of Fig. 1).

with

$$S=\left[2B-C-\sin^2(\theta_i)\right]^{1/2}+2uC^{1/2}\text{arccot}\left\{\left[(u+v)/(u-v)\right]^{1/2}\tan(\theta_i-\Theta/2)\right\}. \tag{10}$$

The time delay Δt between a ray's transit from its entrance plane to its exit plane is

$$\Delta t = L_p/c, \tag{11}$$

where c is the speed of light in the exterior medium. This result will be central for the construction of time domain scattering graphs in [12].

For the special case $2B=C+1$ for an edgeless GLL represented by point α or a point on line segments β and γ of Fig. 1, Eq. (5) for the transmission deflection angle simplifies to

$$\Theta_1=\arccos\left\{\left[1+C\cos(2\theta_i)\right]\Big/\left[1+2C\cos(2\theta_i)+C^2\right]^{1/2}\right\}. \tag{12}$$

This result was also obtained in [9] with $C=1/f^2$ in the notation of that paper. As a mathematical note, the arcsine term in Eq. (5) is always an angle between -90° and $+90^\circ$, thus the branch of the arcsine function to be used is unambiguous. Similarly, the deflection angle in Eq. (12) is always between 180° and 180°, and the branch of the arccosine function to be used is also unambiguous. The expression for S in Eq. (10) does not simplify appreciably for an edgeless particle-like GLL, and thus no counterpart to Eq. (12) is listed here.

The geometry becomes especially simple for the original edgeless Luneburg lens represented by point α. Taking the $C\to 1$ limit of Eqs. (7–10) and (12), the deflection angle is

$$\Theta_1=\theta_i, \tag{13}$$

the shape of the ray path is

$$\rho'^2/\left[2a^2\sin^2(\theta_i/2)\right]+z'^2/\left[2a^2\cos^2(\theta_i/2)\right]=1, \tag{14}$$

and the optical path length from the entrance plane to the exit plane is

$$L_1=a\left[2+\pi/2-\cos(\theta_i)\right]. \tag{15}$$

There is a pleasing analogy between the ray path of the critical ray for total external reflection for a bubble-like GLL in region ν and the grazing incidence ray for an edgeless particle-like GLL. First, when $\theta_i=\theta_i^C$ and $B>C$ in region ν, the ellipse of Eq. (7) lies outside the GLL except at the point where the incident ray tangentially touches the surface, as well as the corresponding point on the other side of the GLL. Thus the transmitted ray path consists of a single point on the surface. This is in analogy to the path of the grazing incidence ray for an edgeless GLL on line segment γ (see Fig. 2c of [9]) which tangentially touches only one point on the sphere surface as it passes it by. Second, when $\theta_i=\theta_i^C$ and $B=C$ in region ν, the ellipse of Eq. (7) degenerates into a circle that coincides with the GLL surface. In analogy to the behavior of the grazing incident ray for an edgeless GLL at point α (see Fig. 2a of [9]), the critical ray in region ν travels 90° on the sphere surface before exiting toward the far-zone. Third, when $\theta_i=\theta_i^C$ and $B<C$ in region ν, the ellipse of Eq. (7) lies everywhere inside the GLL except at the ray's entrance and exit points where it is tangent to the surface. As was the case for a GLL on line segment β (see Fig. 2b of [9]), the ray travels on the interior elliptical path for 180° before exiting the GLL. We will return to this point in [12] when we examine the morphology-dependent resonances of a bubble-like GLL in region ν.

Some of the discontinuities alluded to in Section 2 are now apparent. For example, for the on-axis incident ray with $\theta_i=0^\circ$ the transmission deflection angle is $\Theta_1=0^\circ$ independent of whether the GLL is represented by point α of Fig. 1, a point on line segments β or γ near point α, or a point in region η near line γαβ. But for grazing incidence with $\theta_i=90^\circ$, one has $\Theta_1=0^\circ$ for a point on line segment γ, $\Theta_1=90^\circ$ at point α, $\Theta_1=180^\circ$ for a point on line segment β, and $0^\circ<\Theta_1<180^\circ$ for a point in region η. The value of $\Theta_1(\theta_i=90^\circ)$ has a major impact on the presence or absence of $p=1$ transmission bows. For a point on line segment γ, the derivative $d\Theta_1/d\theta_i$ is positive for $\theta_i=0^\circ$ and it is negative for $\theta_i=90^\circ$, necessitating a relative maximum somewhere in between to change the sign of the slope. The relative maximum is a transmission bow, denoted here by the superscript R. The rainbow scattering angle $\Theta_1^R=\arcsin(C)$ results when $\theta_i^R=\arcsin(B^{1/2})$ as shown in Fig. 3a, b for the special case $B=0.75$, $C=0.5$. The ray trajectories in Fig. 3a show that the near-zone transmission spherical aberration caustic of revolution points toward the sphere – rather than away from it as is the case for the near-zone spherical aberration transmission caustic of a homogeneous sphere. In addition, the outward-pointing arms of the caustic of Fig. 3a evolve into the near-zone rainbow. Fig. 3b shows the deflection angle Θ_1 as a function of the angle of incidence θ_i with its relative maximum. Similarly, for points on line segment β and in region η, $d\Theta_1/d\theta_i$ is positive for both $\theta_i=0^\circ$ and $\theta_i=90^\circ$. For either a point on line segment β or in region η not close to line segment γ, the transmission scattering angle Θ_1 is relatively large for $\theta_i=90^\circ$, the derivative remains positive over the entire θ_i interval, and no transmission bow occurs. But if the GLL in region η is sufficiently close to line segment γ, Θ_1 is relatively small for $\theta_i=90^\circ$ and there is a relative maximum bow that represents a continuation of the relative maximum bow encountered on line segment γ. The derivative turns negative after the relative maximum and requires a relative minimum as is shown in Figs. 3b for $B=0.76$, $C=0.5$ to turn the derivative positive again. This gives rise to two distinct transmission bows in the $p=1$ Debye series channel. Substituting into Eqs. (9) and (10), the relative maximum bow is also a relative maximum of the optical path length, and the relative minimum bow that follows it is also a relative minimum of the optical path length. The presence of two bows in a given p-channel has already been noted for various other refractive index profiles [23,24].

The transmission bow of an edgeless particle-like GLL represented by a point on line segment γ has three notable differences from the well-known one-internal-reflection rainbow of a spherical water droplet. (i) Although a transmission bow (which is also sometimes called Newton's

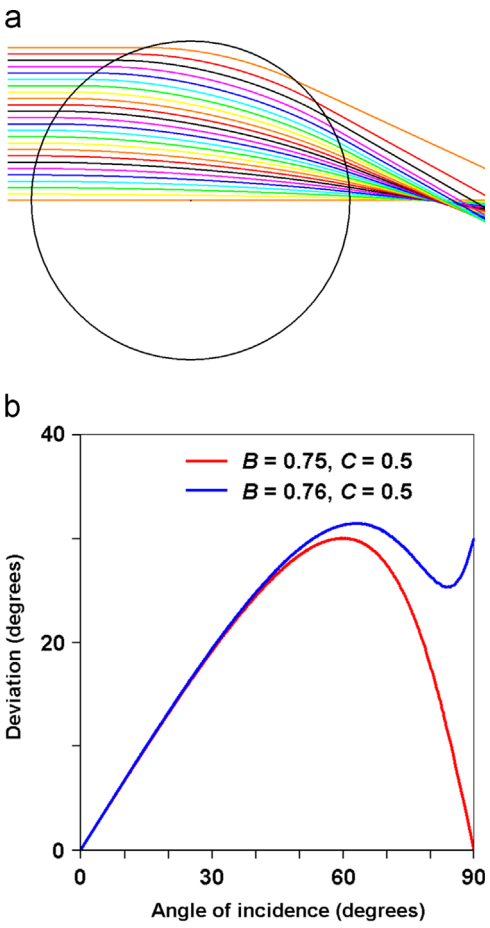

Fig. 3. (a) Ray tracing for a GLL with $B=0.75$ and $C=0.5$, (b) Deviation as a function of angle of incidence θ_i for GLLs with $B=0.75$, $C=0.5$ (on line segment γ of Fig. 1) and $B=0.76$, $C=0.5$ (in region η).

zero-order rainbow [25]) cannot occur for scattering of a plane wave by a homogeneous sphere, it does occur for some particle-like edgeless GLLs. (ii) Although the $p \geq 2$ bows of a homogeneous sphere are a relative minimum of both the scattering angle and the optical path length, the first transmission bow of a GLL is a relative maximum of both. Relative maximum bows are also known for various other radially inhomogeneous refractive index profiles, and are on some occasions associated with the near-onset of the semi-classical effect of orbiting [26,27]. (iii) The rainbows of a homogeneous water sphere are strongly TE polarized because the internal reflection occurs near the Brewster angle which greatly attenuates the TM polarization. In contrast, the transmission bow of an edgeless particle-like GLL occurs equally strongly in both polarizations since no internal reflections are involved.

The scattering angle of the two transmission bows of a hard edge particle-like GLL represented by a point in region η near line segment γ cannot be determined analytically. However, as a specific example of their numerical evaluation, we consider the case of $C=0.50$. Substituting into Eq. (5) we found that when $0.75 < B < 0.773$, $\Theta_1(\theta_i)$ has a broad relative maximum that evolved from the relative maximum of the edgeless GLL with $B=0.75$, $C=0.5$ on line segment γ, and is followed by a narrow relative minimum that occurs for near-grazing incidence. When $B=0.76$, $C=0.5$ in region η, Fig. 3 predicts that the Descartes angle of the relative maximum bow is $\Theta_1=31.43^\circ$ when $\theta_i=63^\circ$ and that of the relative minimum bow is $\Theta_1=25.36^\circ$ when $\theta_i=84^\circ$. As B increases for fixed C, $\Theta_1(\theta_i=90^\circ)$ increases, and the relative maximum and minimum of Θ_1 approach each other and finally coalesce when $B \approx 0.773$. For larger B, $\Theta_1(\theta_i)$ is monotonically increasing and no transmission bow occurs. If the value of B were such that the maximum and minimum bow were near coalescence, the transmission angle Θ_1 would be nearly constant over a relatively large range of incident rays, leading to enhanced scattering at that angle. This was also noted in [28].

The number of $p=1$ bows in the bubble-like region ν is complicated by the fact that as was mentioned earlier, the refracted direction of a light ray at the surface of the Luneburg sphere is opposite to that within the sphere. At the surface Θ_1 curves in the negative angular direction, while inside the sphere it curves in the positive angular direction. The number of $p=1$ bows depends on the interplay between two different conditions. First, $\Theta_1(0)=0$ and

$$\begin{aligned} (\mathrm{d}\Theta_1/\mathrm{d}\theta_i)_{\theta_i=0} &> 0 \quad \text{if} \quad C > 2B-4B^2 \\ &< 0 \quad \text{if} \quad C < 2B-4B^2. \end{aligned} \tag{16}$$

Second, there is a discontinuity in the deflection angle evaluated at θ_i^C

$$\begin{aligned} &\Theta_1(\theta_i^{\,c}) = 2\theta_i^{\,c}-180^\circ \quad \text{if} \quad C < B \\ &2\theta_i^c-90^\circ \quad \text{if} \quad C = B, \\ &2\theta_i^c \quad \text{if} \quad C > B \end{aligned} \tag{17}$$

which was alluded to earlier when the path of the critical ray was described. When $C > 2B-4B^2$ and $C \leq B$ in subregion (i) of region ν in Fig. 4, $\Theta_1(\theta_i)$ starts out being positive and ends up being negative, producing a relative maximum bow. Similarly, when $C < 2B-4B^2$ and $C > B$ in subregion (ii), $\Theta_1(\theta_i)$ starts out being negative and ends up being positive, producing a relative minimum bow. On the other hand, when $C > 2B-4B^2$ and $C > B$ in subregion (iii) or $C < 2B-4B^2$ and $C \leq B$ in subregion (iv), $\Theta_1(\theta_i)$ starts out being positive (negative) and ends up being positive (negative), implying the existence of either zero or two $p=1$ bows. Numerical testing determined that there are two bows for points in subregion (iii) immediately above the $C=B$ line when $0.25 \leq B \leq 0.5$. There are no $p=1$ bows elsewhere in these two portions of region ν. This is exactly what occurred in region η immediately below line segment γ.

As a final note, we only consider transmission bows in detail here because the general rainbow morphology of GLL scattering is already evident at this level. It only remains to be seen how many bows can occur in a given p-channel for various values of B and C. For example, although we have not determined whether three bows can occur in a single $p \geq 2$ channel for a GLL, we have found this to be the case for other specially constructed refractive index profiles that will be published separately.

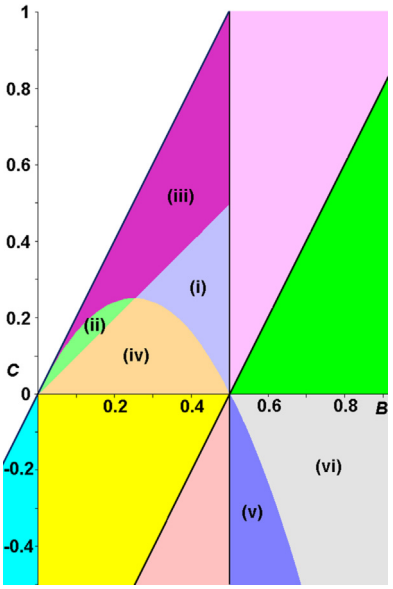

Fig. 4. Sub-divisions of (B, C) parameter space.

3.2. Scattered intensity

The scattered intensity of rays making p–1 internal reflections at the surface of the Luneburg sphere may be obtained using flux conservation [29], giving

$$I_p(\Theta_p) = I_0\left(a^2/R^2\right) T_{21}(\theta_i) R_{11}{}^{p-1}(\theta_i) T_{12}(\theta_i) \left[\sin(\theta_i)\cos(\theta_i)/\sin(\Theta_p)\right] \left|d\Theta_p/d\theta_i\right|^{-1}, \tag{18}$$

where $I_0 = E_0^2/(2\mu_0 c)$, μ_0 is the permeability of free space and R is the far-zone distance of the observation point from the center of the sphere. In addition, T_{21}, R_{11}, and T_{12} are the TE or TM Fresnel intensity coefficients for transmission from the external medium into the sphere, internal reflection, and transmission from the sphere interior to the external medium. When $2B \neq C+1$ for a hard edge particle-like GLL in region η or a hard edge bubble-like GLL in region ν, Eq. (18) can be analytically evaluated in terms of θ_i using Eq. (5). But the result is complicated because the deflection angle function $\Theta_p(\theta_i)$ cannot be analytically inverted for any value of p. However when $2B = C+1$ for an edgeless particle-like GLL (represented by a point on line segments β or γ of Fig. 1), the results simplify greatly because (i) the particle participates in only diffraction and transmission scattering, (ii) the function $\Theta_1(\theta_i)$ is analytically invertible, and (iii) $T_{12}(\theta_i) = T_{21}(\theta_i) = 1$. The transmission deflection angle Θ_1 is a monotonically increasing function of θ_i for a GLL represented by a point on line segment β of Fig. 1. Eq. (12) can then be inverted to give

$$\cos(2\theta_i) = \left\{ -\sin^2(\Theta_1) + \cos(\Theta_1)\left[C^2 - \sin^2(\Theta_1)\right]^{1/2} \right\}/C. \tag{19}$$

Substitution of Eq. (19) into Eq. (18) gives the ray theory transmitted intensity

$$I_1(\Theta_1) = I_0\left(a^2/R^2\right)\left\{ \cos(\Theta_1) + \left[C^2 - \sin^2(\Theta_1)\right]^{1/2} \right\}^2 / \left\{ 4C\left[C^2 - \sin^2(\Theta_1)\right]^{1/2} \right\}. \tag{20}$$

Although these results were reported in [9], they are repeated here in order to provide a comparison with the results of Section 4.2 for an edgeless bubble-like GLL having $C < 0$.

Consider next a GLL represented by a point on line segment γ. Although the deflection angle function $\Theta_1(\theta_i)$ possesses a relative maximum bow, it can be inverted on both supernumerary branches to give

$$\cos(2\theta_i) = \left\{ -\sin^2(\Theta_1) \pm \cos(\Theta_1)\left[C^2 - \sin^2(\Theta_1)\right]^{1/2} \right\}/C, \tag{21}$$

where the upper sign holds for $0^\circ \le \theta_i \le \theta_i^R$ and the lower sign holds for $\theta_i^R \le \theta_i \le 90^\circ$. As was noted in [9], this result is interesting in that for one-internal-reflection scattering by a homogeneous sphere the deflection angle $\Theta_2(\theta_i)$ cannot be analytically inverted on either side of the first order bow. Substituting Eq. (21) into Eq. (18), the ray theory transmitted intensity on either supernumerary branch is

$$I_1(\Theta_1) = I_0\left(a^2/R^2\right)\left\{ \cos(\Theta_1) \pm \left[C^2 - \sin^2(\Theta_1)\right]^{1/2} \right\}^2 / \left\{ 4C\left[C^2 - \sin^2(\Theta_1)\right]^{1/2} \right\}, \tag{22}$$

where the range of θ_i for the upper and lower signs is the same as for Eq. (21). It should be noted that the ray theory intensity of Eq. (22) diverges at Θ_1^R. In addition, both supernumerary branches of $I_1(\Theta_1)$ extend over the full interval $0^\circ \le \Theta_1 \le \Theta_1^R$. This is in contrast to one-internal-reflection scattering by a homogeneous sphere where the smaller impact parameter branch extends over the full interval $\Theta_2^R \le \Theta_2 \le 180^\circ$ in ray theory while the larger impact parameter branch extends only for $\Theta_2^R \le \Theta_2 \le 2\pi - 4\arcsin(1/N)$. Consider lastly the original Luneburg lens represented by point α of Fig. 1. The scattered intensity is [6,9]

$$\begin{array}{ll} I_1(\Theta_1) = I_0\left(a^2/R^2\right)\cos(\Theta_1) & \text{for} \quad 0^\circ \le \Theta_1 \le 90^\circ \\ 0 & \text{for} \quad 90^\circ \le \Theta_1 \le 180^\circ \end{array}. \tag{23}$$

4. Scattering by a Luneburg sphere having $C < 0$

4.1. Deflection angle and properties of the ray path

The mechanical analogy of a GLL with $C < 0$, where the refractive index is an increasing function of r, is a point mass moving in a repulsive external potential. It accelerates away from the force center as it passes by, and the trajectory curves away from the origin. Consistent with this qualitative prediction, the ray path inside a

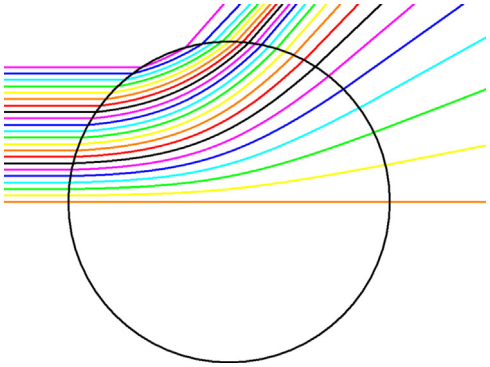

Fig. 5. Ray tracing for a GLL with $B=0.125$ and $C=-0.25$ (in region ξ of Fig. 1).

bubble-like GLL in region ξ or a particle-like GLL in region ψ is found to be a segment of a hyperbola. The hyperbolic path in regions ξ and ψ of Fig. 1 will be seen to be very different from that of region σ. As mentioned previously, this is due to the fact that in region σ the refractive index changes from positive to imaginary at some radius inside the sphere. This point will be discussed later in this section.

We first consider regions ξ and ψ. The transmission deflection angle lies in the interval $-180^\circ \le \Theta_1 \le 0^\circ$ as is shown in Fig. 5 for the special case $B=0.125$, $C=-0.25$ in region ξ. Using the same methods of analysis as in Section 3, the deflection angle for arbitrary $p \ge 1$ is

$$\Theta_p = (p-2)\pi/2 + 2\theta_i + p\,\arcsin\left\{\left[B-\sin^2(\theta_i)\right]/\left[B^2+|C|\sin^2(\theta_i)\right]^{1/2}\right\}. \tag{24}$$

In region ψ, Eq. (24) is valid for all angles of incidence $0^\circ \le \theta_i \le 90^\circ$. But in region ξ it is limited to $0^\circ \le \theta_i \le \theta_i^C$ where the critical angle for total external reflection is given by

$$\sin\left(\theta_i^C\right) = [2B+|C|]^{1/2}. \tag{25}$$

The critical angle limitation applies only to hard-edge bubble-like GLLs in region ξ of Fig. 1 with $2B < C+1$, and not for the edgeless bubble-like GLLs on line δεζ where $2B=C+1$ and Eq. (25) gives $\theta_i^C = 90^\circ$.

For the hyperbolic ray path inside the GLL, the (z', ρ') axes are now rotated clockwise with respect to the (z, ρ) axes by the (positive) angle $-\Theta_1/2$ (since Θ_1 is negative), and the equation of the path inside a GLL is

$$\rho'^2/\left[(v-u)a^2\right] - z'^2/\left[(v+u)a^2\right] = 1, \tag{26}$$

where

$$u = B/|C| \tag{27a}$$

$$v = \left[B^2+|C|\ \sin^2(\theta_i)\right]^{1/2}/|C|. \tag{27b}$$

The point of closest approach of the ray to the origin is again given by $z'=0$ in Eq. (26). The only difference between the ray paths in regions ξ and ψ is that since $N(a)<1$ in region ξ, the ray path is refracted at the sphere surface away from the sphere center before it continues to smoothly curve in the same sense once inside the GLL. On the other hand since $N(a)>1$ in region ψ the ray path initially is refracted at the sphere surface toward the sphere center before it smoothly curves away from the center thereafter. The optical path length of a ray from its entrance plane to its exit plane and that makes p–1 internal reflections within the GLL is given by Eq. (9), but with

$$S = \left[2B+|C|-\sin^2(\theta_i)\right]^{1/2} + 2u|C|^{1/2}\,\mathrm{arccoth}\left\{\left[(v+u)/(v-u)\right]^{1/2}\tan\left(\theta_i - \Theta/2\right)\right\}. \tag{28}$$

For the edgeless bubble-like GLL represented by a point on line segment δ of Fig. 1, Eq. (24) with $p=1$ reduces to

$$\Theta_1 = \arccos\left\{\left[1-|C|\cos(2\theta_i)\right]/\left[1-2|C|\cos(2\theta_i)+|C|^2\right]^{1/2}\right\}. \tag{29}$$

For special case of point ε, the results further simplify to

$$\Theta_1 = \theta_i - \pi/2, \tag{30}$$

$$L_1 = a\left[2-\cos(\theta_i)\right], \tag{31}$$

and the shape of the ray path is

$$\rho'^2/\left[a^2\sin(\theta_i)\right] - z'^2/\left[a^2\sin(\theta_i)\right] = 1, \tag{32}$$

which is shown in Fig. 6.

In Fig. 6 the grazing incidence ray is transmitted in the forward direction. Incident rays with $90^\circ > \theta_i > 0^\circ$ enter the sphere and are deflected by increasingly negative angles. The trajectory of the on-axis ray with $\theta_i = 0^\circ$ has a discontinuous slope at the origin where $N(0)=0$. The incident ray comes in along the –z axis to the origin, turns 90°, and then propagates outward along the ρ axis. This discontinuity is due to the non-physical nature of the refractive index being zero at that point.

The structure of the transmission bows of an edgeless bubble-like GLL represented by a point on either line segment δ or ζ of Fig. 1 is quite similar to that of the edgeless particle-like GLL on line segment γ or β. No bow occurs for a GLL on the line segment ζ, but on the line segment δ the function $\Theta_1(\theta_i)$ has a relative minimum at

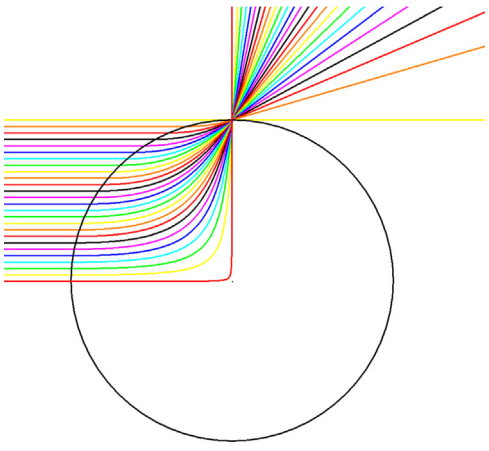

Fig. 6. Ray tracing for a GLL with $B=0$ and $C=-1$ at point ε of Fig. 1.

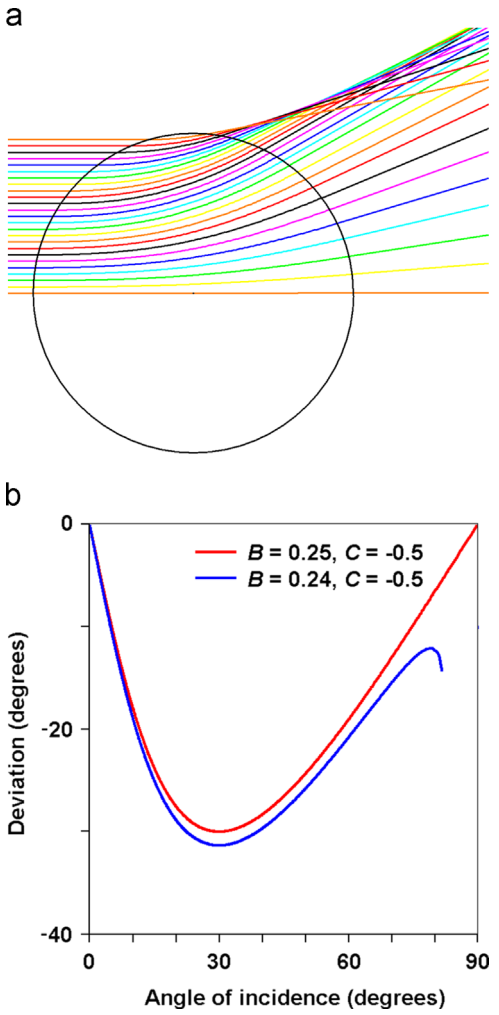

Fig. 7. (a) Ray tracing for a GLL with $B=0.25$ and $C=-0.5$. (b) Deviation as a function of angle of incidence θ_i for GLLs with $B=0.25$, $C=-0.5$ (on line segment δ of Fig. 1) and $B=0.24$, $C=-0.5$ (in region ξ).

the deflection angle $\Theta_1^R=\arcsin(-|C|)$, which occurs when $\theta_i^R=\arcsin(B^{1/2})$ as is shown in Fig.7a, b for the special case of $B=0.25$, $C=-0.50$. Fig. 7a shows the near-zone rainbow caustic in the vicinity of the bubble-like Luneburg sphere. An analogous near-zone behavior occurs for the $p=2$ rainbow of a homogeneous sphere [30], but differs from the near-zone behavior of the rainbow of the particle-like GLL shown in Fig. 3a. Fig. 7b graphs the deflection angle Θ_1 as a function of the angle of incidence θ_i, and shows the rainbow relative minimum.

Substitution into Eq. (28) verifies that the bow is a relative minimum of the optical path length as well. In addition, for a hard edge bubble-like GLL in region ξ, Fig. 7b also shows that if a relative minimum bow occurs that has evolved from that of an edgeless bubble-like GLL on line segment δ, it reverses the sign of $d\Theta_1/d\theta_i$. It thus must be followed by a relative maximum bow occurring for $\theta_i<\theta_i^C$ in order to reverse the sign of the derivative again so that it has the correct sign for the critical angle ray. For the special case of $B=0.25$, $C=-0.5$ on line segment δ, Fig. 7b predicts that the Descartes angle of the relative minimum bow is $\Theta_1=30^\circ$ when $\theta_i=30^\circ$. For $B=0.24$, $C=-0.5$ in region ξ the relative minimum bow has shifted to $\Theta_1=-31.34^\circ$ when $\theta_i=30^\circ$ and the relative maximum bow occurs at $\Theta_1=$-12.14° when $\theta_i=79.1^\circ$. The critical angle for this case is $\Theta_1^C=-15.54^\circ$ when $\theta_i^C=81.85^\circ$.

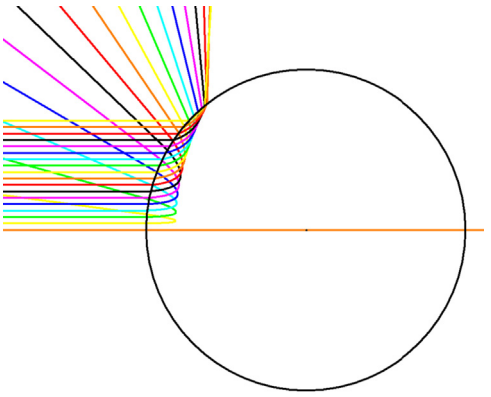

Fig. 8. Ray tracing for a GLL with $B=-0.5$ and $C=-1.5$ (in region σ of Fig. 1).

As was the case in region ν, the number of $p=1$ bows in region ψ is complicated by the fact that the direction of a refracted ray at the sphere surface differs from that within the sphere. In region ψ one has $\Theta_1(0)=0$ and

$$\begin{aligned}(d\Theta_1/d\theta_i)_{\theta i=0}&>0 \quad \text{if} \quad |C|<4B^2-2B\\ &<0 \quad \text{if} \quad |C|>4B^2-2B.\end{aligned} \tag{33}$$

In addition, $\Theta_1(90^\circ)>0$. Thus when $|C|<4B^2-2B$ in subregion (v) of region ψ in Fig. 4, the $p=1$ deflection angle starts out negative and ends up positive, producing a relative minimum bow. When $|C|>4B^2-2B$ in subregion (vi) the deflection angle starts out positive and ends up positive, implying the existence of either zero or two bows. Numerical testing determined that there were no $p=1$ bows.

Finally, we consider a hard edge bubble-like GLL represented by a point in region σ of Fig. 1. The deflection angle of a ray making $p-1$ internal reflections inside the sphere is

$$\Theta_p=(p-2)\pi/2+2\theta_i+p\arcsin\left\{\left[|B|+\sin^2(\theta_i)\right]/\left[|B|^2+|C|\sin^2(\theta_i)\right]^{1/2}\right\}, \tag{34}$$

which for $p=1$ reduces to Eq. (29) the $2B=C+1$ limit on line segment ζ. Again, the angle of incidence is limited to

$$\sin(\theta_i)\le \sin\left(\theta_i^C\right)=[-2|B|+|C|]^{1/2}. \tag{35}$$

Total external reflection occurs at larger angles of incidence, as can be seen in Fig. 8 for $B=-0.5$, $C=-1.5$.

The difference between the shape of the hyperbolic ray paths in Figs. 5 and 8 is now apparent. The transmission angle of the on-axis incident ray is 0° on line segment δ and in region ξ. In the mechanical analogy this is because a particle directly incident on the potential energy hill has

sufficient energy to cross over the top and continue down the other side. But on line segment ζ and in region σ incident rays with small impact parameters penetrate only part way into the sphere before turning around and exiting in the near-backscattering direction. In the mechanical analogy this is because the corresponding point particle does not have enough energy to pass over the top of the potential hill. It travels part way up the hill, momentarily stops, and then travels back down in the direction from which it came. This behavior occurs because in region ξ the refractive index of Eq. (1) is real for $0 \le r \le a$, whereas in region σ it changes from real to imaginary when $r^T = (2|B|/|C|)^{1/2}$. Thus the forward propagation of the ray path inside a GLL in region σ changes from being oscillatory to evanescent at the transition. When $|C| = 2|B|$ for a GLL represented by a point on line segment χ of Fig. 1, the transition T occurs at the sphere surface and the GLL becomes totally reflective.

In region σ the hyperbolic ray path is now

$$\rho'^2/\left[(v+u)a^2\right] - z'^2/\left[(v-u)a^2\right] = 1, \tag{36}$$

where

$$u = |B|/|C| \tag{37a}$$

$$v = \left[|B|^2 + |C|\ \sin^2(\theta_i)\right]^{1/2}/|C|, \tag{37b}$$

and the length of the ray path is given by Eq. (9), but with

$$S = \left[|C| - 2|B| - \sin^2(\theta_i)\right]^{1/2} - 2u|C|^{1/2}\,\mathrm{arccoth}\left\{\left[(v-u)/(v+u)\right]^{1/2}\ \tan(\theta_i - \Theta/2)\right\}. \tag{38}$$

As a mathematical note, Eqs. (24) and (28) and Eqs. (34) and (38) are the analytic continuation of Eqs. (5) and (10) for Θ_p and S from regions η and ν into regions ξ and ψ, and finally into region σ.

4.2. Scattered intensity

As was the case in Section 3.2, the deflection angle function $\Theta_p(\theta_i)$ cannot be analytically inverted for a hard edge bubble-like GLL when $2B \ne C+1$. But for an edgeless GLL with $2B = C+1$, the inversion of $\Theta_1(\theta_i)$ can be analytically accomplished. On line segment ζ of Fig. 1, Eq. (29) can be inverted to give

$$\cos(2\theta_i) = \left\{\sin^2(\Theta_1) - \cos(\Theta_1)\left[|C|^2 - \sin^2(\Theta_1)\right]^{1/2}\right\}/|C|, \tag{39}$$

and the transmitted intensity is

$$I_1(\Theta_1) = I_0\left(a^2/R^2\right)\left\{\cos(\Theta_1) + \left[|C|^2 - \sin^2(\Theta_1)\right]^{1/2}\right\}^2 \Big/ \left\{4|C|\left[|C|^2 - \sin^2(\Theta_1)\right]^{1/2}\right\}. \tag{40}$$

In the $C \to -\infty$ limit, the transmitted intensity on the line segment ζ is asymptotically given by

$$I_1(\Theta_1) \to I_0\left(a^2/4R^2\right), \tag{41}$$

which is identical to that of a perfectively reflective sphere. Instead of the incident rays being reflected at the sphere surface, they penetrate a short distance into the sphere, as is shown in Fig. 8, before reversing direction at the transition T. Although this fulfills the definition of transmission since the rays cross the surface into the sphere and then cross the surface back out again, it blurs the formerly simple intuitive distinction between transmission and external reflection [10]. The ray paths may be interpreted as exhibiting reflection which now occurs a short distance inside the sphere rather than at its surface.

For an edgeless bubble-like GLL represented by a point on the line segment δ of Fig. 1, the deflection angle function may again be inverted on each supernumerary branch to give

$$\cos(2\theta_i) = \left\{\sin^2(\Theta_1) \pm \cos(\Theta_1)\left[|C|^2 - \sin^2(\Theta_1)\right]^{1/2}\right\}/|C|, \tag{42}$$

where the upper and lower signs are the same as for the angle of incidence intervals of Eq. (21). The transmitted intensity is then

$$I_1(\Theta_1) = I_0\left(a^2/R^2\right)\left\{\cos(\Theta_1) \pm \left\{|C|^2 - \sin^2(\Theta_1)\right]^{1/2}\right\}^2 \Big/ \left\{4|C|\left[|C|^2 - \sin^2(\Theta_1)\right]^{1/2}\right\}, \tag{43}$$

with the upper and lower signs being opposite to what they were for the angle of incidence intervals of Eq. (21). Lastly, for the special case of point ε of Fig. 1, the scattered intensity is again given by Eq. (23), but with the intensity being zero for $-180^\circ \le \Theta_1 \le -90^\circ$ and proportional to the cosine function for $-90^\circ \le \Theta_1 \le 0^\circ$.

5. Commentary

For electromagnetic scattering by a sphere, ray theory predicts the existence of a number of divergences or discontinuities, either in the magnitude of the scattered electric field, or in its derivative with respect to scattering angle. In 1959 Ford and Wheeler [26] identified these semi-classical effects to be the rainbow, the glory, and orbiting. In addition, they showed how these divergences are smoothed when the effects of wave scattering are included. Of these, the rainbow and glory occur for scattering by a homogeneous spherical particle, while special properties of the refractive index profile, or equivalently of the potential function in the mechanical analogy, are required for orbiting to occur [26,27]. Since that time, relatively few additional semi-classical effects or smoothing mechanisms have been added to the list. The most noteworthy are the Fock transition that evolves into surface waves when the ray theory scattered intensity for a spherical particle decreases to zero [15,16], and the so-called weak caustic transition in the vicinity of the critical angle for total external reflection for scattering by a spherical bubble in an exterior medium of higher refractive index [31].

In this paper we examined electromagnetic scattering by a class of radially inhomogeneous particles and bubbles known as generalized Luneburg lenses which have the

advantage that ray scattering can be calculated analytically. In doing so, we encountered no new, previously unknown semi-classical scattering effects. On the other hand, we have found several instances in which previously known semi-classical effects appear in a very different way than they do for the familiar situation of scattering by a homogeneous spherical particle or bubble. For example, appealing to the Debye series classification of scattering processes, there can now be two or more bows per p-channel, even including $p=1$ for direct transmission. The bows can now occur for scattering by a bubble as well as scattering by a particle, they can be either a relative maximum or a relative minimum of the deflection angle and ray path, and two rainbows can be made to coalesce, producing especially strong scattering in a given direction. Transmission bows occur equally strongly in both the TE and TM polarization because Brewster angle effects do not occur in the $p=1$ channel, and for edgeless GLLs the appropriate equations are analytically invertible so that the ray scattering intensity for a transmission bow can be expressed directly in terms of the scattering angle Θ_1 rather than indirectly in terms of the angle of incidence θ_i. Lastly, for some parameters there occurs a blurring of the intuitive distinction between exterior reflection and transmission since reflection occurs just beneath the particle surface rather than immediately at it.

As was mentioned in Section 1, scattering by a GLL examined here in ray theory serves as a prototype system for cataloging and understanding the wide range of phenomena that can occur for scattering by a large class of radially inhomogeneous spheres. These scattering phenomena are further examined for a GLL in wave theory and time domain scattering in [12].

References

[1] Gordon JM. Spherical graded-index lenses as perfect imaging and maximum power transfer devices. Appl Opt 2000;39:3825–32.
[2] Pohrivchak MA. Ray- and wave-theoretic approach to electromagnetic scattering from radially inhomogeneous spheres and cylinders. [Ph.D. dissertation]. Old Dominion University; 2014.
[3] Gutman AS. Modified Luneburg lens. J Opt Soc Am 1954;25:855–9.
[4] Garbacz RJ. Electromagnetic scattering from radially inhomogeneous spheres. Proc IRE 1962;50:1837.
[5] Flores JR, Sochacki J, Sochacka M, Staronski R. Quasi-analytical ray tracing through a generalized Luneburg lens. Appl Opt 1992;31:5167–70.
[6] Johnson BR. Light scattering by a multilayer sphere. Appl Opt 1996;35:3286–96.
[7] Sakurai H, Hashidate T, Ohki M, Motojima K, Kozaki S. Electromagnetic scattering by the Luneburg lens reflector. Int J Electron 1988;84:635–45.
[8] Michel F, Reidemeister G, Ohkubo S. Luneburg lens approach to nuclear rainbow scattering. Phys Rev Lett 2002;89:152701.
[9] Lock JA. Scattering of an electromagnetic plane wave by a Luneburg lens. I. Ray theory. J Opt Soc Am A 2008;25:2971–9.
[10] Lock JA. Scattering of an electromagnetic plane wave by a Luneburg lens. II. Wave theory. J Opt Soc Am A 2008;25:2980–90.
[11] Lock JA. Scattering of an electromagnetic plane wave by a Luneburg lens. III. Finely stratified sphere model. J Opt Soc Am A 2008;25:2991–3000.
[12] Laven P, Lock JA, Adam JA. Scattering of a plane electromagnetic wave by a radially-inhomogeneous generalized Luneburg sphere. Part 2: Wave scattering and time-domain scattering. J Quant Spectrosc Radiat Transf 2015;162:164–74.
[13] Olaofe GO, Levine S. Electromagnetic scattering by a spherically symmetric inhomogeneous particle. In: Rowell RL, Stein RS, editors. Electromagnetic scattering. New York: Gordon and Breach; 1967. p. 237–92.
[14] Debye P. Das elektromagnetische feld um einen zylinder und die theorie des regenbogens. Phys Zeit 1908;9:775–78 [Translated into English by Marston PL, editor. Selected papers on geometrical aspects of scattering. SPIE milestone series MS89. Bellingham (WA): SPIE;1994. p. 198–204].
[15] Nussenzveig HM. High-frequency scattering by a transparent sphere. I. Direct reflection and transmission. J Math Phys 1969;10:82–124.
[16] Nussenzveig HM. High-frequency scattering by a transparent sphere. II. Theory of the rainbow and the glory. J Math Phys 1969;10:125–76.
[17] Nussenzveig HM. Diffraction effects in semiclassical scattering. Cambridge (UK): Cambridge University Press; 6.
[18] Marion JB, Thornton ST. Classical dynamics of particles and systems. third ed. San Diego (CA): Harcourt Brace Jovanovich; 1988 [Eq. (8.123)].
[19] Marchand EW. Ray tracing in gradient-index media. J Opt Soc Am 1970;60:1–7.
[20] Marston PL. Critical angle scattering by a bubble: physical-optics approximation and observations. J Opt Soc Am 1979;69:1205–11.
[21] Marston PL, Kingsbury DL. Scattering by a bubble in water near the critical angle: interference effects. J Opt Soc Am 1981;71:192–6.
[22] Kingsbury DL, Marston PL. Mie scattering near the critical angle of bubbles in water. J Opt Soc Am 1981;71:358–61.
[23] Adam JA, Laven P. Rainbows from inhomogeneous transparent spheres: a ray-theoretic approach. Appl Opt 2007;46:922–9.
[24] Adam JA. Zero-order bows in radially inhomogeneous spheres: direct and inverse problems. Appl Opt 2011;50:F50–9.
[25] Bohren CF, Fraser AB. Newton's zero-order rainbow: Unobservable or nonexistent? Am J Phys 1991;59:325–6.
[26] Ford KW, Wheeler JA. Semiclassical description of scattering. Ann Phys 1959;7:259–86.
[27] Berry MV, Mount KE. Semiclassical approximations in wave mechanics. Rep Prog Phys 1972;35:315–97.
[28] Lock JA, Adler CL. Debye-series analysis of the first-order rainbow produced in scattering of a diagonally incident plane wave by a circular cylinder. J Opt Soc Am A 1997;14:1316–28.
[29] van de Hulst HC. Light scattering by small particles. New York: Dover; 203–5.
[30] Nussenzveig HM. The theory of the rainbow. Sci Am 1977;236(4):116–27.
[31] Fiedler-Ferrari N, Nussenzveig HM, Wiscombe WJ. Theory of near-critical angle scattering from a curved surface. Phys Rev A 1991;43:1005–38.